Editors' Suggestion

Supercurrent rectification with time-reversal symmetry broken multiband superconductors

Yuriy Yerin [1], Stefan-Ludwig Drechsler,[2] A. A. Varlamov [1,3] Mario Cuoco [4] and Francesco Giazotto [5]

[1] *CNR-SPIN, via del Fosso del Cavaliere, 100, 00133 Roma, Italy*

[2] *Institute for Theoretical Solid State Physics, Leibniz-Institut für Festkörper- und Werkstoffforschung IFW-Dresden, D-01169 Dresden, Helmholtzstraße 20, Germany*

[3] *Istituto Lombardo "Accademia di Scienze e Lettere", via Borgonuovo, 25-20121 Milan, Italy*

[4] *CNR-SPIN, c/o Universitá di Salerno, I-84084 Fisciano (SA), Italy*

[5] *NEST Istituto Nanoscienze-CNR and Scuola Normale Superiore, I-56127 Pisa, Italy*

(Received 19 April 2024; revised 11 July 2024; accepted 15 July 2024; published 2 August 2024)

We consider nonreciprocal supercurrent effects in Josephson junctions based on multiband superconductors with a pairing structure that can break time-reversal symmetry. We demonstrate that a nonreciprocal supercurrent can be generally achieved by the cooperation of interband superconducting phase mismatch and interband scattering as well as by multiband phase frustration. The effect of interband impurity scattering indicates that the amplitude and sign of the nonreciprocal supercurrent are sensitive to the interband phase relation. For the case of a three-band superconductor, due to phase frustration, we show that the profile of the supercurrent rectification is marked by a hexagonal pattern of nodal lines with vanishing amplitude. Remarkably, around the nodal lines, the supercurrent rectification amplitude exhibits threefold structures with an alternating sign. We show that the hexagonal pattern and the threefold structure in the interband phase space turn out to be dependent on the tunneling amplitude of each band. These findings provide hallmarks of the supercurrent rectification which can be potentially employed to unveil the occurrence of spin-singlet multiband superconductivity with time-reversal symmetry breaking.

DOI: 10.1103/PhysRevB.110.054501

I. INTRODUCTION

Nonreciprocal effects in superconductors are generally based on phenomena where the amplitude of the supercurrent depends on the direction of its flow. The rectification of the supercurrent is then a direct result of the nonreciprocal superconducting transport. Recently, a large body of works has been devoted to the achievement of supercurrent rectification [1–8] both motivated by fundamental questions on the underlying generating mechanisms as well as on the technological challenges regarding the development of dissipationless electronics and quantum circuits [9]. Nonreciprocal supercurrent phenomena, apart from conventional superconductors, indeed, have been successfully demonstrated in several materials including noncentrosymmetric superconductors [1,10–12], two-dimensional electron gases and polar semiconductors [13], patterned superconductors [14], superconductor-magnet hybrids [4,15], Josephson junctions with magnetic atoms [16] and quantum dots [17], twisted graphene systems [18], and high T_c superconductors [7,8].

Several mechanisms, either intrinsic or extrinsic in nature, have been proposed to devise a supercurrent diode with control of the rectification in sign and amplitude. In this context it is generally accepted that breaking of time-reversal and inversion symmetries is a key requirement for achieving a nonreciprocal supercurrent. For instance, Cooper-pair momenta [18–20] or helical phases [21–27], as well as screening currents [28,29], and supercurrents related to self-induced field [30,31] have been considered as physical scenarios and mechanisms to get nonreciprocal supercurrent effects. The breaking of time-reversal symmetry is mostly achieved through external magnetic fields. Vortices are also expected to yield supercurrent diode effects and their role has been investigated for a variety of physical configurations [13,31–40]. Proposals of magnetic field-free superconducting diodes have been using magnetic materials in suitably designed heterostructures [4,15]. Instead, back-action supercurrent mechanisms and electrical gating [41,42] can result in superconducting rectification effects without the use of external magnetic fields or magnetic materials.

In this context, the exploitation of an unconventional superconducting state with intrinsic time-reversal symmetry breaking represents a potential path to get supercurrent rectification. This is indeed an open problem which has not been fully explored yet. The role of symmetry broken phases in the normal state and the occurrence of time-reversal broken superconducting phases have been addressed only for two-dimensional materials demonstrating that indeed they can lead to a distinct type of supercurrent rectification without the need of external magnetic fields [43].

Several superconducting materials exhibit signatures of spontaneous time-reversal symmetry breaking (TRSB) below the transition temperature [44–46]. In this type of superconductors the occurrence of internal magnetic fields is either due to the magnetic moment of the Cooper pairs, as in nonunitary spin-triplet pairing, or by the multicomponent nature of the superconducting condensate in multiband superconductors. For the latter, it is the complex superposition of distinct order parameters that leads to a breaking of the time-reversal symmetry. In this context, it is known that

disorder can facilitate the formation of time-reversal symmetry broken phases both in multiband superconductors [47–51]. In particular, for spin-singlet multiband superconductors a distinct role is played by the so-called π pairing, i.e., the antiphase relation between the order parameters in different bands or, equivalently, the sign reversal of the Josephson coupling between Cooper pairs in different bands. Apart from the connection with the time-reversal symmetry breaking, the intertwinning of π pairing and multiband electronic structure often marks the occurrence of unconventional superconducting phases, e.g., in iron-based [52,53] and oxide interface superconductors [54,55], electrically or orbitally driven superconductivity [56–60], and multiband noncentrosymmetric superconductors [54,61–63]. Understanding the mechanisms for time-reversal symmetry broken multiband phases as well as identifying specific detection schemes for accessing the complexity of multiband superconductors are key challenges not yet fully settled.

In this paper, we consider multiband superconductors that can break the time-reversal symmetry due to nontrivial interband phase relation and we study the character of nonreciprocal supercurrent effects. We demonstrate that nonreciprocal supercurrent in Josephson junctions with multiband superconductors can be generally achieved by exploiting the combination of the interband superconducting phase mismatch and the strength of the interband scattering. In particular, we find that the effect of interband impurity scattering can help to distinguish among a dominant 0 or π pairing in the superconductor. We show that distinct variations in the amplitude and sign of the rectification amplitude can be observed as a function of the interband impurity scattering strength. In the case of three-band superconductors there is a phase frustration in the complex superposition of the order parameters that results in the formation of nodal lines or large regions in the parameter space with vanishing rectification amplitude. The nodal patterns are marked by multifold structures with sign changes of the rectification amplitude. The location and shape of these structures depend on the tunneling amplitudes.

The paper is organized as follows. In Sec. II we present supercurrent nonreciprocal effects in a Josephson junction combining single- and two-band superconductors with time-reversal symmetry breaking pairing by focusing on the role of interband impurity scattering. Section III is devoted to a multiband phase frustrated configuration. There, we present the study of a Josephson junction hosting a three-band superconductor interfaced with a convectional single-band superconductor. The conclusions are given in Sec. IV.

II. JOSEPHSON CURRENT BETWEEN A SINGLE-BAND AND A TWO-BAND SUPERCONDUCTOR

In this section, we demonstrate how the interplay of interband impurity scattering and nontrivial interband phase can yield supercurrent nonreciprocal effects. This is done by considering a Josephson junction composed of a conventional single-band superconductor interfaced to an unconventional superconductor with two bands whereas the time-reversal symmetry breaking arises from the nontrivial interband superconducting phase relation.

Let us start with the description of the unconventional two-band superconductor in the presence of impurity scattering and zero magnetic field. In the dirty limit the Eilenberger formalism for a two-band superconductor, as for the conventional single-band s-wave counterpart, can be reduced to the Usadel equations for quasiclassical Green's functions decomposed in spherical harmonics [64]:

$$\omega f_i - D_i(g_i\nabla^2 f_i - f_i\nabla^2 g_i) = \Delta_i g_i + \Gamma_{ij}(g_i f_j - g_i f_j), \quad (1)$$

where $f_i = f_i(\mathbf{r},\omega)$, $g_i = g_i(\mathbf{r},\omega)$ are the $\mathbf{r}$ coordinate-dependent anomalous and normal quasiclassical Green's functions connected by the standard normalization condition ${g_i}^2 + |f_i|^2 = 1$, $\{i, j\} = 1, 2$. The remaining notations are as follows: $\omega \equiv \omega_n = (2n+1)\pi T$ is the Matsubara frequency, D_i are the intraband diffusion coefficients caused by the intraband elastic scattering, Δ_i represent complex order parameters in a two-band superconductor. Finally, Γ_{ij} denote the interband scattering coefficients, which are absent in the case of a clean multiband superconductor. When $\Gamma_{ij} = 0$, Eq. (1) can be decoupled and the Green's functions of different bands are related only through the interband interaction in the self-consistency equations for the order parameters.

To determine the supercurrent, Eq. (1) must be evaluated together with the expression for the current density

$$j(\mathbf{r}) = -e\pi \mathrm{i} T \sum_i \sum_\omega N_i D_i (f_i^* \nabla f_i - f_i \nabla f_i^*), \quad (2)$$

where N_i corresponds to the partial contribution of each band to the density of states at the Fermi level.

A. The model and main equations

Now, we proceed with the study of the properties of the Josephson junction between the standard single-band superconductor (left lead) and the unconventional multiband one with the TRSB state (right lead). The Josephson junction is studied as a weak link connecting two superconducting leads in the form of a thin short filament of length L, which in turn is an extension of the multiband superconductor. Based on the condition that the length $L \lesssim \min \xi_i(T)$ being the temperature-dependent coherence lengths one can consider Josephson junction as a quasi-one-dimensional system and neglect all terms in Eq. (1) except the gradient one [65]

$$g_i \frac{d^2}{dx^2} f_i - f_i \frac{d^2}{dx^2} g_i = 0. \quad (3)$$

Equation (3) can be solved using the parametrized functions Φ_i which are connected with the Green's functions f_i and g_i by the following expressions (see, e.g., Ref. [66]):

$$g_i = \frac{\omega}{\sqrt{\omega^2 + \Phi_i \Phi_i^*}}, \quad f_i = \frac{\Phi_i}{\sqrt{\omega^2 + \Phi_i \Phi_i^*}}, \quad \Phi_i = \frac{\omega f_i}{g_i}. \quad (4)$$

With this parametrization the normalization conditions for the Green functions are fulfilled automatically. We notice that in the single-band superconducting lead of the Josephson junction at $x = -L/2$ the function $\Phi_0 = \Delta_0$. Here and hereafter the zero subscript is attributed to the parameters of the left side of the Josephson junction. Furthermore, we suppose that the critical temperature $T_c^{(s)}$ of the bulk

conventional single-band superconducting bank of the Josephson junction is at least not less than that of the bulk multiband superconductor $T_c^{(m)}$, i.e., it will be assumed that the $T_c^{(s)} \geqslant T_c^{(m)}$, where the upper indices s and m emphasize the belonging to a conventional single-band and an unconventional TRSB multi-band superconductor, respectively [67]. Although this condition imposes considerable restrictions on the list of superconducting materials that can be used to implement this type of diode, nevertheless, the most suitable and promising compound for the role of a multicomponent (effective two-band) superconductor with broken time-reversal symmetry can be $Ba_xK_{1-x}Fe_2As_2$. As experiments have shown [68], at the doping level $x \approx 0.73$ a state with broken time-reversal symmetry emerges in this superconductor, with the critical temperature $T_c^{(m)} \approx 10$ K. In view of this, s-wave single-band counterpart of the Josephson junction can be niobium nitride NbN with $T_c^{(s)} \approx 16$ K or some compounds from superconducting A15 family (as V_3Si with $T_c^{(s)} \approx 16$ K) or even clean two-band superconducting magnesium diboride MgB_2 with $T_c^{(s)} \approx 39$ K, in which both components of the order parameter have an isotropic s-wave structure without the presence of the TRSB state. In any case, it is important to note that the Josephson junction must remain always superconducting, i.e., none of the ingredients of the diode enter the normal state at the given temperature chosen for the calculations.

The Josephson phase φ, which we define as the difference between the phases of the order parameter Δ_0 of the single-band superconductor (left lead) and the order parameter Δ_1 of the multiband superconductor (right lead), determines the boundary condition

$$\Delta_0(-L/2) = |\Delta_0| \exp(-i\varphi/2). \tag{5}$$

Now let us determine the boundary conditions for the Green's functions in Eq. (3) for the two-band superconducting bank (at $x = L/2$). They can be found in the homogeneous expressions of Eqs. (1) where the gradient terms are now being ignored. In general case, there is no analytical solution for $\Gamma_{ij} \neq 0$. However, close to $T_c^{(m)}$ an amenable conjecture for the Green's functions can be found by the method of successive approximations over the moduli of the order parameters Δ_i, which yields [47]

$$f_1^{(0)}(L/2) = \frac{(\omega + \Gamma_{21})\Delta_1 + \Gamma_{12}\Delta_2}{\omega(\omega + \Gamma_{12} + \Gamma_{21})},$$
$$f_2^{(0)}(L/2) = \frac{(\omega + \Gamma_{12})\Delta_2 + \Gamma_{21}\Delta_1}{\omega(\omega + \Gamma_{12} + \Gamma_{21})}, \tag{6}$$

and

$$f_1^{(1)}(L/2) = \frac{\Gamma_{12}(\omega + \Gamma_{21})(\Delta_1 - \Delta_2)\left|f_2^{(0)}\right|^2 - [((\omega + \Gamma_{21})^2 + \Gamma_{12}(\omega + 2\Gamma_{21}))\Delta_1 + \Gamma_{12}(\omega + \Gamma_{12})\Delta_2]\left|f_1^{(0)}\right|^2}{\omega(\omega + \Gamma_{12} + \Gamma_{21})},$$
$$f_2^{(1)}(L/2) = \frac{\Gamma_{21}(\omega + \Gamma_{12})(\Delta_2 - \Delta_1)\left|f_1^{(0)}\right|^2 - [((\omega + \Gamma_{12})^2 + \Gamma_{21}(\omega + 2\Gamma_{12}))\Delta_2 + \Gamma_{21}(\omega + \Gamma_{21})\Delta_1]\left|f_2^{(0)}\right|^2}{\omega(\omega + \Gamma_{12} + \Gamma_{21})}. \tag{7}$$

In Eqs. (6) and (7) the values of the order parameters on the right side of the junction are

$$\Delta_1(L/2) = |\Delta_1| \exp(i\varphi/2) \tag{8}$$

and

$$\Delta_2(L/2) = |\Delta_2| \exp(i\varphi/2 + i\phi). \tag{9}$$

Here ϕ is the intrinsic difference between the phases of the order parameters of the two-band superconductor that can attain nonzero values due to the presence of the interband scattering ($\Gamma_{ij} \neq 0$) solely [47,48,69,70]. In the absence of the latter, the values of ϕ can be equal to 0 or π depending on the attractive or repulsive nature of the interband interaction and corresponds to s_{++} or $s_{\pm}$ pairing symmetry, respectively. Otherwise, for ϕ different from 0 or π, a two-band superconductor is characterized by a complex superposition of the two order parameters that thus breaks the time-reversal symmetry.

We notice that the solutions for the anomalous Green's functions cannot be used for the entire temperature range of superconducting state since the applicability of Eqs. (6) and (7) is restricted by the region where both $|\Delta_i|$ are small, i.e., nearby the critical temperature $T_c^{(m)}$. In turn, the latter depends not only on the intraband and interband interactions but also on the interband scattering rate $\Gamma = \Gamma_{12} = \Gamma_{21}$ (with the additional assumption of the equal density of states at the Fermi level for each of the bands $N_1 = N_2$), which lowers the value of $T_c^{(m)}$ as compared to the critical temperature $T_{c0}^{(m)}$ of a clean two-band superconductor when $\Gamma = 0$ [47,64]. Correspondingly, our study of the current-phase relations will be performed for temperatures close enough to the $T_c^{(m)}$ of the dirty two-band superconductor (see Appendix B and Fig. 6 therein).

B. Current-phase relations and the diode effect

Equations (3) with boundary conditions (6) and (7) admit an analytical solution. Substituting the solutions of Eqs. (3) to (2) for the current density we derive the explicit expression for the Josephson current flowing between the single-band and the dirty two-band superconductor (see details of the derivation in Appendix A):

$$I(\varphi) = \frac{\pi T}{e} \sum_i \frac{1}{R_{Ni}} \sum_\omega \frac{C_i}{\sqrt{1 - \kappa_i^2 + C_i^2}} \times \left[\arctan\left(\frac{\omega\kappa_i C_i + \Phi_i^-(\kappa^2 - 1)}{\omega\sqrt{\kappa_i^2 - C_i^2 - 1}} \right) - \arctan\left(\frac{\omega\kappa_i C_i + \Phi_0^-(\kappa^2 - 1)}{\omega\sqrt{\kappa_i^2 - C_i^2 - 1}} \right) \right]. \tag{10}$$

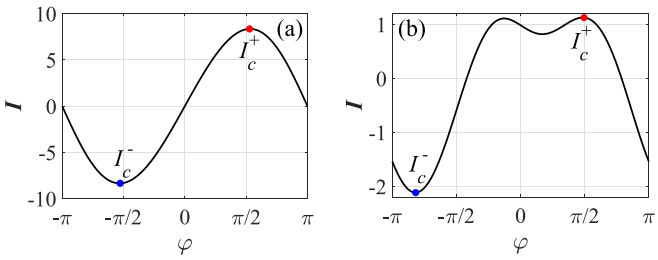

FIG. 1. Current-phase relation for the Josephson junction between a single-band and an s_{++} two-band superconductor with (a) $\Gamma = 0$ and $\phi = 0$ and an $s_\pm + is_{++}$ two-band superconductor with representative values of the interband scattering $\Gamma \approx 0.062 T_{c0}^{(m)}$, and the interband phase difference $\phi \approx \frac{3}{25}\pi$ (b). We employ representative values of the order parameters in the two-band superconductors: $|\Delta_1| = 2|\Delta_0|$, $|\Delta_2| = 3|\Delta_0|$ at $T = 0.7\, T_{c0}^{(m)}$. The amplitude of the supercurrent I is taken in units of $\frac{\pi|\Delta_0|}{eR_{N1}}$.

Here the Josephson phase difference φ enters implicitly via the functions

$$\kappa_i = \frac{\Phi_0^+ - \Phi_i^+}{\Phi_0^- - \Phi_i^-}, \tag{11}$$

$$C_i = \frac{\Phi_0^- \Phi_i^+ - \Phi_0^+ \Phi_i^-}{\omega(\Phi_0^- - \Phi_i^-)}, \tag{12}$$

where

$$\Phi_0^\pm = \tfrac{1}{2}(\Phi_0 \pm \Phi_0^*), \quad \Phi_i^\pm = \tfrac{1}{2}(\Phi_i \pm \Phi_i^*), \tag{13}$$

and R_{Ni} are partial contributions to the junction's resistance (also referred as Sharvin resistance for the case of point contacts [71]). In the following, we assume $R_{N1} = R_{N2} = R_{N3}$.

For the case of Josephson junction between two different s-wave single-band superconductors, Eq. (10) yields the current-phase relation already obtained in Ref. [72]. Another important remark is that the derivation of Eq. (10) was done in the single-channel limit for a disordered regime of diffusive type for the Josephson junction.

Using Eq. (10) one can plot the current-phase relation $I(\varphi)$ of the Josephson junction between a single-band superconductor and a two-band superconductor with the s_{++} [Fig. 1(a)] and the chiral order-parameter pairing, i.e., $s_{+-} + is_{++}$ [see Fig. 1(b)]. For the sake of clarity, in these figures we introduce the notation of the critical current I_c^+ (filled red dot) for the maximum forward supercurrent and I_c^- (filled blue dot) for the maximum negative amplitude of the supercurrent.

As one can see from Fig. 1(a) in the case of s_{++} pairing symmetry, when $\phi = 0$ and $\Gamma = 0$, the current-phase relation is symmetric and the supercurrent exhibits a reciprocal behavior [73,74]. As expected, this behavior is qualitatively consistent with that one of the Josephson junction between two different single-band s-wave superconductors separated by a very thin normal layer [72] or to the that of standard Josephson junction with constriction (S-c-S type) [65,75]. For this pairing state the forward (I_c^+) and backward (I_c^-) critical currents of the junction are identical, i.e., $I_c^+ = I_c^-$.

The current-phase relation is substantially different when considering the effect of interband scattering assuming a complex superposition of 0 and π pairing order parameters (i.e., $s_\pm + is_{++}$). First of all, as one can see from Fig. 1(b) that the current-phase relation $I(\varphi)$ becomes nonsinusoidal, in contrast to the similar pattern in Fig. 1(a). Moreover, it has the asymmetry of the so-called φ_0 Josephson junction, i.e., at $\varphi = 0$ the supercurrent amplitude is not zero [76,77]. Another remarkable feature of this current-phase relation is that for specific values of Γ and the intrinsic phase difference ϕ, the critical currents I_c^+ and I_c^- of the Josephson junction can be substantially different in amplitude, with I_c^+ which can be even become identically zero.

Such an unusual asymmetric pattern of the current-phase relation in Josephson junction hosting a single-band and a two-band superconductor opens the path for achieving nonreciprocal supercurrent effects guided by multiband time-reversal symmetry broken phases. The corresponding diode rectification amplitude η can be determined by evaluating the difference among the maximal amplitudes of the critical currents for forward (I_c^+) and backward (I_c^-) flow directions:

$$\eta = \frac{I_c^+ - |I_c^-|}{I_c^+ + |I_c^-|}. \tag{14}$$

We start by observing that the rectification amplitude for the current-phase relation as shown in Fig. 1(a) is $\eta = 0$ ($I_c^+ = |I_c^-|$) while that one corresponding to Fig. 1(b) can reach the value $\eta \approx -0.3$. One can then track the evolution of the current-phase relation and within the non-self-consistent approach extract the corresponding rectification amplitudes for any value of the interband phase difference ϕ and interband scattering rate Γ. The outcome of this analysis is reported in Fig. 2. We find that the rectification amplitude has a distinct dependence on the interband scattering rate when comparing the pairing configuration at $\phi < \pi/4$ with that close to $\phi \sim \pi$. Indeed, in the former region, close to 0-interband pairing coupling, the rectification amplitude of the supercurrent is negligible below a critical threshold for the interband scattering rate Γ. Then, the increase of Γ leads to a growth of the rectification amplitude and a subsequent sign reversal with equally sized rectification states. To additionally emphasize these statements, we make cross sections of the phase diagram in Fig. 2(a) for some fixed values of Γ. The results of these cross sections in the form of $\eta(\phi)$ dependencies are presented in Fig. 2(b).

By inspection of the current-phase relation across the transition, one can grasp the origin of the achieved rectification. This is due to the occurrence of a 0-to-π Josephson phase transition that is marked by a sign change of the odd-parity first-harmonic component. It is known that, in general, the supercurrent rectification value is sizable when the first and second harmonics are comparable in amplitude [78]. For this reason, since the second-harmonic component is typically smaller than the first harmonic when approaching the 0-to-π phase transition we have that the first and second harmonics get similar amplitude.

It is worth noting that for two-band superconductors with s_{++}- ($\phi = 0$ or equivalently $\phi = 2\pi$) or $s_\pm$-wave ($\phi = \pi$) symmetry of the order parameter the diode effect does not occur even in the presence of impurities.

We point out that, in principle, for the constructed phase diagram of the superconducting diode rectification amplitude, of

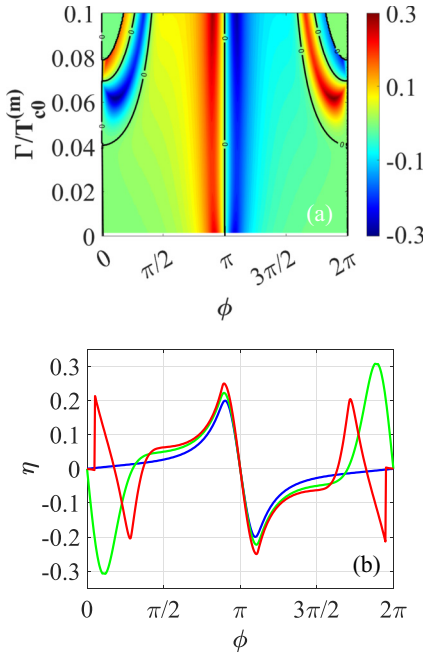

FIG. 2. (a) Contour map of the supercurrent rectification amplitude η for the Josephson junction as a function of the phase difference ϕ and the interband scattering rate $\Gamma/T_{c0}^{(m)}$ assuming a two-band superconductor with $|\Delta_1| = 2|\Delta_0|$, $|\Delta_2| = 3|\Delta_0|$ at $T = 0.7T_{c0}^{(m)}$. η is determined by evaluating the difference among the maximal amplitude of the critical currents for forward (I_c^+) and backward (I_c^-) flow directions as in Eq. 14. (b) Cross sections of the color map shown in (a) as a function of rectification amplitude η versus the phase difference ϕ for different values of the $\Gamma = 0.02T_{c0}^{(m)}$ (blue line), $\Gamma = 0.0617T_{c0}^{(m)}$ (green line), and $\Gamma = 0.08T_{c0}^{(m)}$ (red line).

course, only the states with a phase difference ϕ different from zero in a two-band superconductor can be realized only when $\Gamma \neq 0$. Therefore, the lower parts of the diagram adjacent to the ϕ axis are limiting cases that cannot be physically achieved when Γ is vanishing. To underline this feature, we intentionally depict the lower part in Fig. 2(a) as a white area. However, as can be seen in Fig. 2, the highest rectification amplitude η is attained away from the above-mentioned region of the phase diagram. Moreover, there can be other mechanisms to get a nontrivial phase difference ϕ due to intraband and interband interaction [see, for instance, Eq. (7) in Ref. [47] or Eq. (9) in Ref. [70]]. A detailed justification of our non-self-consistent approach for the calculation of η is presented in Appendix B, where we also provide the schematic and the comparative treatment with the fully self-consistent analysis.

III. JOSEPHSON CURRENT BETWEEN A SINGLE-BAND AND A THREE-BAND SUPERCONDUCTOR

The replacement of the two-band superconductor by a three-band counterpart in the Josephson junction leads to additional phase interference effects and, as a consequence, yields a different structure in the current-phase relation [74,79–82] as well as frustration effects in the dynamics [83]. Since the Josephson current is now determined by three partial contributions instead of two, for convenience and clarity, we exclude the effect of interband scattering and set

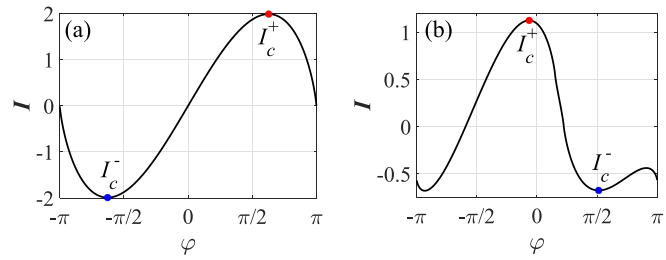

FIG. 3. Current-phase relations for the Josephson junction between single- and three-band superconductor with $\phi = \theta = 0$ (a) and $\phi \approx 1.22$, $\theta \approx 1.33$ (in radians) (b) for $|\Delta_1| = |\Delta_2| = |\Delta_3| = |\Delta_0|$ at $T = 0$. Current is measured in units of $\frac{\pi|\Delta_0|}{eR_{N1}}$.

$\Gamma_{ij} = 0$, i.e., we consider a dirty three-band superconductor with a strong enough dominant intraband scattering as compared to its interband counterparts.

Equation (10) remains applicable for the given Josephson system with the only correction now for the contribution to the current from the third band of the three-band superconductor. Based on the assumption $\Gamma_{ij} = 0$ one can find an exact expression for the boundary conditions without the necessity of solving Eqs. (1) by the method of successive approximations like in a two-band case. Here, boundary conditions acquire the form

$$\Phi_0(-L/2) = |\Delta_0| \exp(-i\varphi/2) \tag{15}$$

for the left lead (single-band superconductor) and

$$\begin{aligned} \Phi_1(L/2) &= |\Delta_1| \exp(i\varphi/2), \\ \Phi_2(L/2) &= |\Delta_2| \exp(i\varphi/2 + i\phi), \\ \Phi_3(L/2) &= |\Delta_3| \exp(i\varphi/2 + i\theta) \end{aligned} \tag{16}$$

for the right bank (three-band superconductor). The intrinsic phase differences ϕ and θ correspond to the pairs of order parameters Δ_1, Δ_2 and Δ_1, Δ_3 of a bulk three-band superconductor [84].

To avoid cumbersome expressions we further assume the coincidence of the order-parameter amplitude in superconducting leads: $|\Delta_0| = |\Delta_1| = |\Delta_2| = |\Delta_3|$. Moreover, bearing in mind that in the case under consideration we deal with the exact solutions of Eqs. (1) for Green's functions, we can treat the case at zero temperature by summing over Matsubara frequencies in Eq. (10). The resulting Josephson current is given by the following expression:

$$\begin{aligned} I(\varphi) = {} & \frac{\pi|\Delta_0|}{eR_{N1}} \cos\frac{\varphi}{2} \operatorname{Artanh}\left[\sin\frac{\varphi}{2}\right], \\ & + \frac{\pi|\Delta_0|}{eR_{N2}} \cos\left(\frac{\varphi}{2} + \phi\right) \operatorname{Artanh}\left[\sin\left(\frac{\varphi}{2} + \phi\right)\right], \\ & + \frac{\pi|\Delta_0|}{eR_{N3}} \cos\left(\frac{\varphi}{2} + \theta\right) \operatorname{Artanh}\left[\sin\left(\frac{\varphi}{2} + \theta\right)\right]. \end{aligned} \tag{17}$$

Equation (17) can be regarded as a generalization of the classical formula, derived by Kulik and Omelyanchouk for the S-c-S contact at $T = 0$ [65,75], for the case of the Josephson junction between the conventional s-wave and three-band superconductor. As expected [Fig. 3(a)] at $\phi = 0$ and $\theta = 0$ and the critical currents turn out to be reciprocal: $I_c^+ = |I_c^-|$.

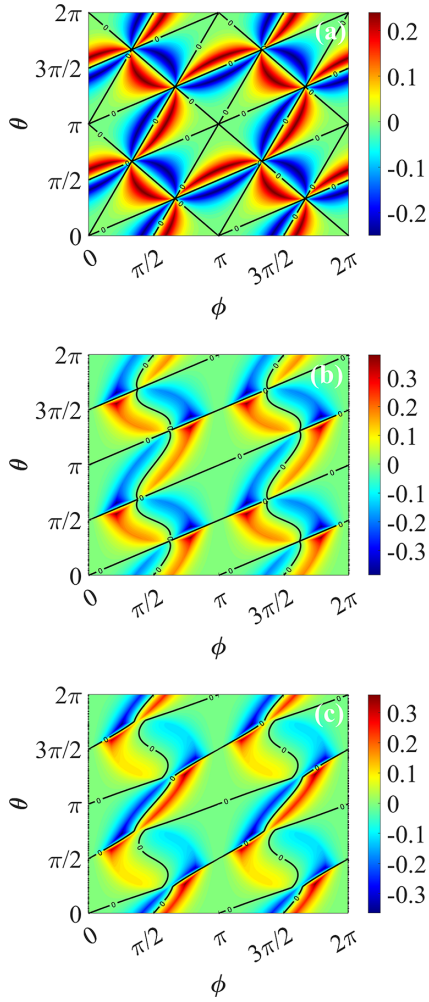

FIG. 4. Diode rectification amplitude of the Josephson junction between a single-band and a three-band superconductor as a function of phases differences in a three-band superconductor for (a) $R_{N1} = R_{N2} = R_{N3}$, (b) $R_{N1}/R_{N2} = 1$, $R_{N1}/R_{N3} = 2$, and (c) $R_{N1}/R_{N2} = 2$, $R_{N1}/R_{N3} = 3$ at zero temperature.

Instead, for the three-band superconductor with a time-reversal broken order parameter (when ϕ and θ are different from zero and/or π), the current-phase relation exhibits a complex nonsinusoidal pattern [Fig. 3(b)]. Indeed, one can observe that for certain values of the intrinsic phase differences $\{\phi, \theta\}$ a strong asymmetry of critical currents is achieved [Fig. 3(b)]. There, the profile of the current-phase relation presented in Fig. 3(b) can provide a sizable rectification value $\eta \approx 0.25$.

The overall rectification amplitude of the Josephson junction with three-band superconducting lead is reported in Fig. 4 for different cases of band-dependent tunneling amplitude by scanning the whole space of interband phase relation. In Fig. 4(a) the symmetric case with all the bands having the same resistance is shown. The profile of the rectification can be understood by inspection of the harmonic content of the current-phase relation in Eq. (17). Indeed, at $\phi = \pi/3$ and $\theta = \pi/6 + (2n+1)\frac{\pi}{2}$ (for $n = 1, 2, \dots$) all the even harmonic components are vanishing. Hence, the rectification amplitude is zero because the current-phase relation has a fixed parity. Since the parity of the current-phase relation cannot be fixed in isolated points of the phase space there must be nodal lines. Indeed, along the lines defined by the relation $\theta = (2n+1)\pi/2 + \phi$, $\theta = (2n+1)\pi/2 + \phi$, $\theta = n\pi - \phi$, the even harmonics of the second and third terms of Eq. (17) cancel out. This implies that the rectification amplitude has to vanish. Since the rectification amplitude can be maximized when the first- and the second-harmonics components have comparable amplitude we expect that moving away from the nodal lines there will be regions where the rectification increases. This is indeed a feature of the pattern of the rectification amplitude [Fig. 4(a)] with phase space domains of sizable rectification strength developing around the nodal lines. A modification of the tunneling amplitude R_N alters the balance between the terms which are dependent on θ and ϕ leading to a variation of the nodal lines [Fig. 4(a)] and of the rectification pattern around them. To make the behavior of the nodal lines clearer, we take cross sections of the phase diagrams in Fig. 4 for a given value of the phase difference θ. For this purpose, we fix $\theta = \pi/3$ so that in the case of equal partial contributions to the Josephson-junction resistance, the cross section passes through the intersection points of the nodal lines. Figure 5 shows the evolution of the dependence of the rectification amplitude η as a function of phase difference ϕ at $\theta = \pi/3$ for the same resistance contributions as in Figs. 4(a)–4(c).

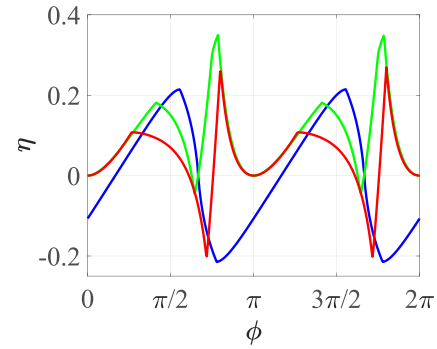

FIG. 5. Diode rectification amplitude of the Josephson junction between a single-band and a three-band superconductor as a function of phase difference ϕ in a three-band superconductor with the fixed value of the phase difference $\theta = \pi/3$ for $R_{N1} = R_{N2} = R_{N3}$ (blue line), $R_{N1}/R_{N2} = 1$, $R_{N1}/R_{N3} = 2$ (green line), and $R_{N1}/R_{N2} = 2$, $R_{N1}/R_{N3} = 3$ (red line) at zero temperature.

Finally, we point out that for the diagram in Fig. 4, the states close to $\theta = 0$ and $\phi = 0$ lines do not fulfill the stability conditions and are metastable configurations [84]. The same arguments apply for the states $\{\phi = 0, \theta = 0\}$, $\{\phi = 0, \theta = \pi\}$, $\{\phi = \pi, \theta = 0\}$, $\{\phi = \pi, \theta = \pi\}$. For other points of the phase diagram it is instead possible to set the intraband and interband interactions (elements of 3×3 matrix), which satisfy the conditions of achieving a stable ground state.

As a final remark, we would like to note that this model can be generalized to the case of a larger number of order parameters in a multiband superconductor. We do not present here the diagram of a superconducting diode for the case of a pure n-band superconductor because of technical difficulties in its visualization. However, it is obvious that in this case the rectification amplitude pattern becomes even more nontrivial.

IV. CONCLUSIONS

The effects of nonreciprocal supercurrent in Josephson junctions have been studied using multiband superconductors that can disrupt time-reversal symmetry by interband phase reconstruction. It has been shown that nonreciprocal supercurrent can be achieved through a combination of interband superconducting phase mismatch and scattering, as well as by exploiting multiband phase frustration. The presence of impurity scattering between bands affects the magnitude and direction of the nonreciprocal supercurrent, depending on the interband phase relationship. In the case of a three-band superconductor with a phase-frustrated configuration, the supercurrent rectification profile is characterized by a hexagonal pattern of nodal lines with zero amplitude. Interestingly, the amplitude of supercurrent rectification shows a three-fold pattern with alternating signs around the nodal lines. We have found that the hexagonal pattern and the threefold structure in the interband phase space are influenced by the band-dependent tunneling amplitudes. These findings applied to corresponding diodes can be used to detect a state with the time-reversal symmetry breaking in multiband superconductors due to a nontrivial interband phase relation.

Finally, we point out that the behavior of the junction with three-band superconductor interfaced to a one-band superconductor can be also mimicked by designing a double-loop superconducting quantum interference device. Indeed, recently a double-loop interferometer based on conventional superconductor-normal-superconductor weak links has been demonstrated to yield a rectification hosting nodal lines and multifold sign tunable patterns [85]. We argue that the use of such double-loop interference device based on multiband superconductors can be employed to disentangle the interband phase complexity. Also, we believe that our findings provide new functionalities for superconducting electronics.

ACKNOWLEDGMENTS

M.C. and F.G. acknowledge financial support from the EUs Horizon 2020 Research and Innovation Framework Program under Grant Agreement No. 964398 (SUPERGATE) and from PNRR MUR Project No. PE0000023-NQSTI. M.C. acknowledges support from the QUANCOM Project No. 225521 (MUR PON Ricerca e Innovazione Grant No. 20142020 ARS01 00734). F.G. acknowledges the EUs Horizon 2020 Research and Innovation Framework Programme under Grant No. 101057977 (SPECTRUM) for partial financial support.

APPENDIX A: DERIVATION OF THE EXPRESSION FOR THE JOSEPHSON CURRENT

By means of parametrization given by Eq. (4), simplified Usadel equations (3) can be reduced to their first integrals

$$\frac{1}{\omega}g_i^2\frac{\partial\Phi_i^+}{\partial x}=A_i,\quad \frac{1}{\omega}g_i^2\frac{\partial\Phi_i^-}{\partial x}=B_i, \tag{A1}$$

where A and B are integration constants, and we recall that

$$g_i^2=\frac{\omega^2}{\omega^2+(\Phi_i^+)^2-(\Phi_i^-)^2} \tag{A2}$$

and

$$\Phi_i^{\pm}=\tfrac{1}{2}(\Phi_i+\Phi_i^*). \tag{A3}$$

Comparison of Eqs. (A1) yields the equality

$$A_i\frac{\partial\Phi_i^-}{\partial x}=B_i\frac{\partial\Phi_i^+}{\partial x}. \tag{A4}$$

From Eq. (A4) it follows

$$\Phi_i^+=\kappa_i\Phi_i^-+\omega C_i, \tag{A5}$$

where $\kappa_i=\frac{A_i}{B_i}$ and C are integration constants.

Now we can substitute Eq. (A5) into (A1) and solve the first-order differential equation for $\Phi_i^-(x)$, which gives

$$\Phi_i^-=-\frac{C_i\kappa_i\omega}{\kappa_i^2-1}+\frac{\omega\sqrt{\kappa_i^2-C_i^2-1}}{\kappa_i^2-1}\times\tan\left[\sqrt{\kappa_i^2-C_i^2-1}\left(B_ix+x_i^{(0)}\right)\right] \tag{A6}$$

and using again Eq. (A5) we get the solution also for

$$\Phi_i^+=-\frac{C_i\omega}{\kappa_i^2-1}+\frac{\omega\kappa_i\sqrt{\kappa_i^2-C_i^2-1}}{\kappa_i^2-1}\times\tan\left[\sqrt{\kappa_i^2-C_i^2-1}\left(B_ix+x_i^{(0)}\right)\right], \tag{A7}$$

where $x_i^{(0)}$ is the integration constant.

To find all constants, we apply the boundary conditions (5), (8), and (9) and obtain systems of corresponding equations

$$\begin{aligned}
\Phi_0^-&=-\frac{C_1\kappa_1\omega}{\kappa_1^2-1}+\frac{\omega\sqrt{\kappa_1^2-C_1^2-1}}{\kappa_1^2-1}\tan\left[\sqrt{\kappa_1^2-C_1^2-1}\left(-B_1\frac{L}{2}+x_1^{(0)}\right)\right],\\
\Phi_0^+&=-\frac{C_1\omega}{\kappa_1^2-1}+\frac{\omega\kappa_1\sqrt{\kappa_1^2-C_1^2-1}}{\kappa_1^2-1}\tan\left[\sqrt{\kappa_1^2-C_1^2-1}\left(-B_1\frac{L}{2}+x_1^{(0)}\right)\right],\\
\Phi_1^-&=-\frac{C_1\kappa_1\omega}{\kappa_1^2-1}+\frac{\omega\sqrt{\kappa_1^2-C_1^2-1}}{\kappa_1^2-1}\tan\left[\sqrt{\kappa_1^2-C_1^2-1}\left(B_1\frac{L}{2}+x_1^{(0)}\right)\right],\\
\Phi_1^+&=-\frac{C_1\omega}{\kappa_1^2-1}+\frac{\omega\kappa_2\sqrt{\kappa_1^2-C_1^2-1}}{\kappa_1^2-1}\tan\left[\sqrt{\kappa_1^2-C_1^2-1}\left(B_1\frac{L}{2}+x_1^{(0)}\right)\right]
\end{aligned} \tag{A8}$$

and

$$\Phi_0^- = -\frac{C_2\kappa_2\omega}{\kappa_2^2-1} + \frac{\omega\sqrt{\kappa_2^2-C_2^2-1}}{\kappa_2^2-1}\tan\left[\sqrt{\kappa_2^2-C_2^2-1}\left(-B_2\frac{L}{2}+x_2^{(0)}\right)\right],$$

$$\Phi_0^+ = -\frac{C_2\omega}{\kappa_2^2-1} + \frac{\omega\kappa_2\sqrt{\kappa_2^2-C_2^2-1}}{\kappa_2^2-1}\tan\left[\sqrt{\kappa_2^2-C_2^2-1}\left(-B_2\frac{L}{2}+x_2^{(0)}\right)\right],$$

$$\Phi_2^- = -\frac{C_2\kappa_2\omega}{\kappa_2^2-1} + \frac{\omega\sqrt{\kappa_2^2-C_2^2-1}}{\kappa_2^2-1}\tan\left[\sqrt{\kappa_2^2-C_2^2-1}\left(B_2\frac{L}{2}+x_2^{(0)}\right)\right],$$

$$\Phi_2^+ = -\frac{C_2\omega}{\kappa_2^2-1} + \frac{\omega\kappa_2\sqrt{\kappa_2^2-C_2^2-1}}{\kappa_2^2-1}\tan\left[\sqrt{\kappa_2^2-C_2^2-1}\left(B_2\frac{L}{2}+x_2^{(0)}\right)\right]. \tag{A9}$$

After long but straightforward calculations we have the solutions for eight constants:

$$C_i = \frac{\Phi_0^-\Phi_i^+ - \Phi_0^+\Phi_i^-}{\omega(\Phi_0^- - \Phi_i^-)}, \tag{A10}$$

$$\kappa_i = \frac{\Phi_0^+ - \Phi_i^+}{\Phi_0^- - \Phi_i^-}, \tag{A11}$$

$$B_i = \frac{1}{L\sqrt{\kappa_i^2-C_i^2-1}}\left[\arctan\left(\frac{\omega\kappa_i C_i + \Phi_i^-(\kappa_i^2-1)}{\omega\sqrt{\kappa_i^2-C_i^2-1}}\right) - \arctan\left(\frac{\omega\kappa_i C_i + \Phi_0^-(\kappa_i^2-1)}{\omega\sqrt{\kappa_i^2-C_i^2-1}}\right)\right], \tag{A12}$$

$$x_i^{(0)} = \frac{1}{2}\frac{1}{\sqrt{\kappa_i^2-C_i^2-1}}\left[\arctan\left(\frac{\omega\kappa_i C_i + \Phi_i^-(\kappa_i^2-1)}{\omega\sqrt{\kappa_i^2-C_i^2-1}}\right) + \arctan\left(\frac{\omega\kappa_i C_i + \Phi_0^-(\kappa_i^2-1)}{\omega\sqrt{\kappa_i^2-C_i^2-1}}\right)\right]. \tag{A13}$$

Substitution of Eqs. (A6) and (A7) into the expression for the current density (2) leads to

$$j = -2i\pi T\sum_i N_i D_i \sum_\omega B_i C_i. \tag{A14}$$

After that, Eq. (A14) for the current density can be transformed into the expression for the current, which finally results in Eq. (10).

APPENDIX B: A BRIEF DESCRIPTION OF THE SELF-CONSISTENT APPROACH

A self-consistent approach implies that the Usadel equations (1) and the expression for the current density (2) must be supplemented by the equation for order parameters Δ_i, which we did not involve into our consideration here:

$$\Delta_i = 2\pi T\sum_j\sum_{\omega>0}^{\langle\omega_0\rangle}\lambda_{ij}f_j, \tag{B1}$$

where λ_{ij} is the matrix of intraband ($i=j$) and interband ($i\neq j$) coupling constants and $\langle\omega_0\rangle$ is the cutoff frequency.

As it was shown already for the case of a bulk homogeneous two-band superconductor, when gradient terms are excluded from the consideration in Eqs. (1), the Usadel equations admit approximated solutions (6) and (7). Subsequent substitution of these solutions to the self-consistent equation (B1) allows to derive an internal phase difference between the order parameters [47,70]

$$\cos\phi = -\frac{a_{12}+c_{11}|\Delta_1|^2+c_{22}|\Delta_2|^2}{2c_{12}|\Delta_1||\Delta_2|}, \tag{B2}$$

where coefficients are expressed as

$$a_{12} = -N_1\left(\frac{\lambda_{12}}{\det\lambda_{ij}} + 2\pi T\sum_{\omega>0}^{\omega_c}\frac{\Gamma_{12}}{\omega(\omega+\Gamma_{12}+\Gamma_{21})}\right), \tag{B3}$$

$$c_{ii} = N_i\pi T\sum_{\omega>0}^{\omega_c}\frac{\Gamma_{ij}(\omega+\Gamma_{ji})[\omega^2+(\omega+\Gamma_{ji})(\Gamma_{ij}+\Gamma_{ji})]}{\omega^3(\omega+\Gamma_{ij}+\Gamma_{ji})^4}, \tag{B4}$$

and

$$c_{12} = N_1\pi T\sum_{\omega>0}^{\omega_c}\frac{\Gamma_{12}(\omega+\Gamma_{12})(\omega+\Gamma_{21})(\Gamma_{12}+\Gamma_{21})}{\omega^3(\omega+\Gamma_{12}+\Gamma_{21})^4}. \tag{B5}$$

Also, the expression for the critical temperature as a function of the impurity scattering rate Γ can be obtained within the linearized Usadel equations (1) taking into account Eq. (B1) [64]. Here we only provide the final result of calculations showing the suppression of the critical temperature $T_c^{(m)}$ with respect to the critical temperature $T_{c0}^{(m)}$ of a clean two-band superconductor without impurities, i.e., when $\Gamma = \Gamma_{12} = \Gamma_{21} = 0$:

$$U\left(\frac{\Gamma}{\pi T_c^{(m)}}\right) = -\frac{2[w\lambda\,\ln t + \lambda(\lambda_{11}+\lambda_{22}) - 2w]\ln t}{2w\lambda\,\ln t + \lambda(\lambda_{11}+\lambda_{22}-\lambda_{12}-\lambda_{21}) - 2w}, \tag{B6}$$

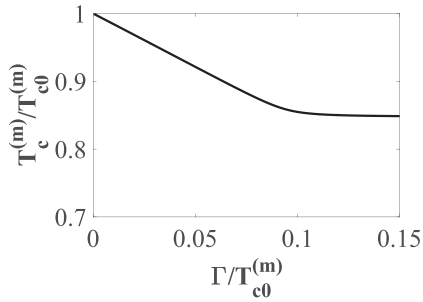

FIG. 6. The critical temperature $T_c^{(m)}$ of a dirty two-band superconductor as a function of the interband scattering rate Γ with $\lambda_{11} = 0.35$, $\lambda_{22} = 0.347$, $\lambda_{12} = \lambda_{21} = -0.01$. The values of $T_c^{(m)}$ and Γ are calibrated to the critical temperature of a two-band superconductor without impurities $T_{c0}^{(m)}$ and $\Gamma = 0$, respectively.

where the new function is introduced $U(x) = \psi(\frac{1}{2} + x) - \psi(\frac{1}{2})$ expressed via the digamma function $\psi(x)$, $t = T_c^{(m)}/T_{c0}^{(m)}$ and where λ is the largest eigenvalue of the matrix of intraband and interband coefficients and $w = \det \lambda_{ij} = \lambda_{11}\lambda_{22} - \lambda_{12}\lambda_{21}$. The numerical solution of the transcendental equation (B6) is presented in Fig. 6.

Within the self-consistent approach one can consider a certain two-band superconductor with given values of microscopic constants λ_{ij}. Then by setting the value of the microscopic interband scattering coefficient $\Gamma = \Gamma_{12} = \Gamma_{21}$ (also, assuming for simplicity $N_1 = N_2$) one can compute the values of the order-parameter moduli $|\Delta_1|$, $|\Delta_2|$ and the intrinsic phase difference ϕ. After that, the rectification amplitude of the diode η can be immediately evaluated based on the current-phase relation (10).

In our non-self-consistent approach, the value of the interband scattering coefficient and the intrinsic phase difference is captured already in the phase diagram in Fig. 2 to get a certain value of the rectification amplitude η. Also, we fix the values of $|\Delta_1|$ and $|\Delta_2|$ with respect to the modulus of the order parameter of the single-band superconductor $|\Delta_0|$. This means that now our consideration is converting into a search for the unknown microscopic parameters of a corresponding two-band superconductor, namely, four interaction constants (two intraband λ_{11}, λ_{22} and two interband λ_{12}, λ_{21}) and the modulus of the order parameter of the single-band superconductor, through which the moduli of the order parameter of the two-band counterpart have been determined before.

Thus, we have five unknown variables and three equations, two of which stem from Eq. (B1) for the order parameters by substituting known expressions for the anomalous Green's functions [see Eqs. (6) and (7)] and one for the phase difference (B2). Eventually, there is an underdetermined system of equations, which allows us to freely speculate about the fixed so far values Γ and ϕ for a certain unconventional two-band superconductor in order to satisfy given value of the rectification amplitude η. In other words, the phase diagram in Fig. 2 is not plotted for any particular two-band superconductor as an element of a Josephson diode, but for different unconventional two-band superconductors.

[1] F. Ando, Y. Miyasaka, T. Li, J. Ishizuka, T. Arakawa, Y. Shiota, T. Moriyama, Y. Yanase, and T. Ono, Observation of superconducting diode effect, Nature (London) **584**, 373 (2020).

[2] L. Bauriedl, C. Bäuml, L. Fuchs, C. Baumgartner, N. Paulik, J. M. Bauer, K.-Q. Lin, J. M. Lupton, T. Taniguchi, K. Watanabe, C. Strunk, and N. Paradiso, Supercurrent diode effect and magnetochiral anisotropy in few-layer $NbSe_2$, Nat. Commun. **13**, 4266 (2022).

[3] C. Baumgartner, L. Fuchs, A. Costa, S. Reinhardt, S. Gronin, G. C. Gardner, T. Lindemann, M. J. Manfra, P. E. Faria Junior, D. Kochan, J. Fabian, N. Paradiso, and C. Strunk, Supercurrent rectification and magnetochiral effects in symmetric Josephson junctions, Nat. Nanotechnol. **17**, 39 (2022).

[4] H. Wu, Y. Wang, Y. Xu, P. K. Sivakumar, C. Pasco, U. Filippozzi, S. S. P. Parkin, Y.-J. Zeng, T. McQueen, and M. N. Ali, The field-free Josephson diode in a van der Waals heterostructure, Nature (London) **604**, 653 (2022).

[5] K.-R. Jeon, J.-K. Kim, J. Yoon, J.-C. Jeon, H. Han, A. Cottet, T. Kontos, and S. S. P. Parkin, Zero-field polarity-reversible Josephson supercurrent diodes enabled by a proximity-magnetized Pt barrier, Nat. Mater. **21**, 1008 (2022).

[6] M. Nadeem, M. S. Fuhrer, and X. Wang, The superconducting diode effect, Nat. Rev. Phys. **5**, 558 (2023).

[7] S. Y. F. Zhao, X. Cui, P. A. Volkov, H. Yoo, S. Lee, J. A. Gardener, A. J. Akey, R. Engelke, Y. Ronen, R. Zhong, G. Gu, S. Plugge, T. Tummuru, M. Kim, M. Franz, J. H. Pixley, N. Poccia, and P. Kim, Time-reversal symmetry breaking superconductivity between twisted cuprate superconductors, Science **382**, 1422 (2023).

[8] S. Ghosh, V. Patil, A. Basu, Kuldeep, A. Dutta, D. A. Jangade, R. Kulkarni, A. Thamizhavel, J. F. Steiner, F. von Oppen, and M. M. Deshmukh, High-temperature Josephson diode, Nat. Mater. **23**, 612 (2024).

[9] R. Upadhyay, D. S. Golubev, Y.-C. Chang, G. Thomas, A. Guthrie, J. T. Peltonen, and J. P. Pekola, Microwave quantum diode, Nat. Commun. **15**, 630 (2024).

[10] R. Wakatsuki, Y. Saito, S. Hoshino, Y. M. Itahashi, T. Ideue, M. Ezawa, Y. Iwasa, and N. Nagaosa, Nonreciprocal charge transport in noncentrosymmetric superconductors, Sci. Adv. **3**, e1602390 (2017).

[11] E. Zhang, X. Xu, Y.-C. Zou, L. Ai, X. Dong, C. Huang, P. Leng, S. Liu, Y. Zhang, Z. Jia, X. Peng, M. Zhao, Y. Yang, Z. Li, H. Guo, S. J. Haigh, N. Nagaosa, J. Shen, and F. Xiu, Nonreciprocal superconducting $NbSe_2$ antenna, Nat. Commun. **11**, 5634 (2020).

[12] J. Hasan, D. Shaffer, M. Khodas, and A. Levchenko, Supercurrent diode effect in helical superconductors, Phys. Rev. B **110**, 024508 (2024).

[13] Y. M. Itahashi, T. Ideue, Y. Saito, S. Shimizu, T. Ouchi, T. Nojima, and Y. Iwasa, Nonreciprocal transport in gate-induced polar superconductor $SrTiO_3$, Sci. Adv. **6**, eaay9120 (2020).

[14] Y.-Y. Lyu, J. Jiang, Y.-L. Wang, Z.-L. Xiao, S. Dong, Q.-H. Chen, M. V. Milošević, H. Wang, R. Divan, J. E. Pearson, P. Wu, F. M. Peeters, and W.-K. Kwok, Superconducting diode effect via conformal-mapped nanoholes, Nat. Commun. **12**, 2703 (2021).

[15] H. Narita, J. Ishizuka, R. Kawarazaki, D. Kan, Y. Shiota, T. Moriyama, Y. Shimakawa, A. V. Ognev, A. S. Samardak, Y. Yanase, and T. Ono, Field-free superconducting diode effect in noncentrosymmetric superconductor/ferromagnet multilayers, Nat. Nanotechnol. **17**, 823 (2022).

[16] M. Trahms, L. Melischek, J. F. Steiner, B. Mahendru, I. Tamir, N. Bogdanoff, O. Peters, G. Reecht, C. B. Winkelmann, F. von Oppen, and K. J. Franke, Diode effect in Josephson junctions with a single magnetic atom, Nature (London) **615**, 628 (2023).

[17] D. Debnath and P. Dutta, Gate-tunable Josephson diode effect in Rashba spin-orbit coupled quantum dot junctions, Phys. Rev. B **109**, 174511 (2024).

[18] J.-X. Lin, P. Siriviboon, H. D. Scammell, S. Liu, D. Rhodes, K. Watanabe, T. Taniguchi, J. Hone, M. S. Scheurer, and J. I. A. Li, Zero-field superconducting diode effect in small-twist-angle trilayer graphene, Nat. Phys. **18**, 1221 (2022).

[19] B. Pal, A. Chakraborty, P. K. Sivakumar, M. Davydova, A. K. Gopi, A. K. Pandeya, J. A. Krieger, Y. Zhang, M. Date, S. Ju, N. Yuan, N. B. M. Schröter, L. Fu, and S. S. P. Parkin, Josephson diode effect from Cooper pair momentum in a topological semimetal, Nat. Phys. **18**, 1228 (2022).

[20] N. F. Q. Yuan and L. Fu, Supercurrent diode effect and finite-momentum superconductors, Proc. Natl. Acad. Sci. USA **119**, e2119548119 (2022).

[21] V. M. Edelstein, Magnetoelectric effect in polar superconductors, Phys. Rev. Lett. **75**, 2004 (1995).

[22] K. Samokhin, Symmetry and topology of noncentrosymmetric superconductors, Ann. Phys. **359**, 385 (2015).

[23] K. V. Samokhin and S. P. Mukherjee, Fermionic boundary modes in two-dimensional noncentrosymmetric superconductors, Phys. Rev. B **94**, 104523 (2016).

[24] S. Ilić and F. S. Bergeret, Theory of the supercurrent diode effect in Rashba superconductors with arbitrary disorder, Phys. Rev. Lett. **128**, 177001 (2022).

[25] A. Daido and Y. Yanase, Superconducting diode effect and nonreciprocal transition lines, Phys. Rev. B **106**, 205206 (2022).

[26] J. J. He, Y. Tanaka, and N. Nagaosa, A phenomenological theory of superconductor diodes, New J. Phys. **24**, 053014 (2022).

[27] B. Turini, S. Salimian, M. Carrega, A. Iorio, E. Strambini, F. Giazotto, V. Zannier, L. Sorba, and S. Heun, Josephson diode effect in high-mobility InSb nanoflags, Nano Lett. **22**, 8502 (2022).

[28] Y. Hou, F. Nichele, H. Chi, A. Lodesani, Y. Wu, M. F. Ritter, D. Z. Haxell, M. Davydova, S. Ilić, O. Glezakou-Elbert, A. Varambally, F. S. Bergeret, A. Kamra, L. Fu, P. A. Lee, and J. S. Moodera, Ubiquitous superconducting diode effect in superconductor thin films, Phys. Rev. Lett. **131**, 027001 (2023).

[29] A. Sundaresh, J. I. Väyrynen, Y. Lyanda-Geller, and L. P. Rokhinson, Diamagnetic mechanism of critical current nonreciprocity in multilayered superconductors, Nat. Commun. **14**, 1628 (2023).

[30] V. M. Krasnov, V. A. Oboznov, and N. F. Pedersen, Fluxon dynamics in long Josephson junctions in the presence of a temperature gradient or spatial nonuniformity, Phys. Rev. B **55**, 14486 (1997).

[31] T. Golod and V. M. Krasnov, Demonstration of a superconducting diode-with-memory, operational at zero magnetic field with switchable nonreciprocity, Nat. Commun. **13**, 3658 (2022).

[32] D. Suri, A. Kamra, T. N. G. Meier, M. Kronseder, W. Belzig, C. H. Back, and C. Strunk, Non-reciprocity of vortex-limited critical current in conventional superconducting micro-bridges, Appl. Phys. Lett. **121**, 102601 (2022).

[33] A. Gutfreund, H. Matsuki, V. Plastovets, A. Noah, L. Gorzawski, N. Fridman, G. Yang, A. Buzdin, O. Millo, J. W. A. Robinson, and Y. Anahory, Direct observation of a superconducting vortex diode, Nat. Commun. **14**, 1630 (2023).

[34] W. Gillijns, A. V. Silhanek, V. V. Moshchalkov, C. J. O. Reichhardt, and C. Reichhardt, Origin of reversed vortex ratchet motion, Phys. Rev. Lett. **99**, 247002 (2007).

[35] J. Jiang, Y.-L. Wang, M. V. Milošević, Z.-L. Xiao, F. M. Peeters, and Q.-H. Chen, Reversible ratchet effects in a narrow superconducting ring, Phys. Rev. B **103**, 014502 (2021).

[36] A. He, C. Xue, and Y.-H. Zhou, Switchable reversal of vortex ratchet with dynamic pinning landscape, Appl. Phys. Lett. **115**, 032602 (2019).

[37] D. Margineda, A. Crippa, E. Strambini, Y. Fukaya, M. T. Mercaldo, M. Cuoco, and F. Giazotto, Sign reversal diode effect in superconducting dayem nanobridges, Commun. Phys. **6**, 343 (2023).

[38] F. Paolucci, G. De Simoni, and F. Giazotto, A gate- and flux-controlled supercurrent diode effect, Appl. Phys. Lett. **122**, 042601 (2023).

[39] A. Greco, Q. Pichard, and F. Giazotto, Josephson diode effect in monolithic dc-SQUIDs based on 3D Dayem nanobridges, Appl. Phys. Lett. **123**, 092601 (2023).

[40] J. Lustikova, Y. Shiomi, N. Yokoi, N. Kabeya, N. Kimura, K. Ienaga, S. Kaneko, S. Okuma, S. Takahashi, and E. Saitoh, Vortex rectenna powered by environmental fluctuations, Nat. Commun. **9**, 4922 (2018).

[41] D. Margineda, A. Crippa, E. Strambini, Y. Fukaya, M. T. Mercaldo, C. Ortix, M. Cuoco, and F. Giazotto, Back-action supercurrent diodes, arXiv:2311.14503.

[42] R. Seoane Souto, M. Leijnse, C. Schrade, M. Valentini, G. Katsaros, and J. Danon, Tuning the Josephson diode response with an ac current, Phys. Rev. Res. **6**, L022002 (2024).

[43] H. D. Scammell, J. I. A. Li, and M. S. Scheurer, Theory of zero-field superconducting diode effect in twisted trilayer graphene, 2D Mater. **9**, 025027 (2022).

[44] C. Kallin and J. Berlinsky, Chiral superconductors, Rep. Prog. Phys. **79**, 054502 (2016).

[45] K. I. Wysokiski, Time reversal symmetry breaking superconductors: Sr_2RuO_4 and beyond, Condens. Matter **4**, 47 (2019).

[46] S. K. Ghosh, M. Smidman, T. Shang, J. F. Annett, A. D. Hillier, J. Quintanilla, and H. Yuan, Recent progress on superconductors with time-reversal symmetry breaking, J. Phys.: Condens. Matter **33**, 033001 (2021).

[47] V. Stanev and A. E. Koshelev, Complex state induced by impurities in multiband superconductors, Phys. Rev. B **89**, 100505(R) (2014).

[48] J. Garaud, A. Corticelli, M. Silaev, and E. Babaev, Properties of dirty two-band superconductors with repulsive interband

interaction: Normal modes, length scales, vortices, and magnetic response, Phys. Rev. B **98**, 014520 (2018).
[49] W.-C. Lee, S.-C. Zhang, and C. Wu, Pairing state with a time-reversal symmetry breaking in FeAs-based superconductors, Phys. Rev. Lett. **102**, 217002 (2009).
[50] S. Maiti, M. Sigrist, and A. Chubukov, Spontaneous currents in a superconductor with $s+is$ symmetry, Phys. Rev. B **91**, 161102(R) (2015).
[51] K. V. Samokhin, Ginzburg-Landau energy of multiband superconductors with interband pairing, Phys. Rev. B **109**, 134508 (2024).
[52] V. Grinenko, R. Sarkar, K. Kihou, C. H. Lee, I. Morozov, S. Aswartham, B. Büchner, P. Chekhonin, W. Skrotzki, K. Nenkov, R. Hühne, K. Nielsch, S.-L. Drechsler, V. L. Vadimov, M. A. Silaev, P. A. Volkov, I. Eremin, H. Luetkens, and H.-H. Klauss, Superconductivity with broken time-reversal symmetry inside a superconducting *s*-wave state, Nat. Phys. **16**, 789 (2020).
[53] V. Grinenko, D. Weston, F. Caglieris, C. Wuttke, C. Hess, T. Gottschall, I. Maccari, D. Gorbunov, S. Zherlitsyn, J. Wosnitza, A. Rydh, K. Kihou, C.-H. Lee, R. Sarkar, S. Dengre, J. Garaud, A. Charnukha, R. Hühne, K. Nielsch, B. Büchner *et al.*, State with spontaneously broken time-reversal symmetry above the superconducting phase transition, Nat. Phys. **17**, 1254 (2021).
[54] M. S. Scheurer and J. Schmalian, Topological superconductivity and unconventional pairing in oxide interfaces, Nat. Commun. **6**, 6005 (2015).
[55] G. Singh, C. Guarcello, E. Lesne, D. Winkler, T. Claeson, T. Bauch, F. Lombardi, A. D. Caviglia, R. Citro, M. Cuoco, and A. Kalaboukhov, Gate-tunable pairing channels in superconducting non-centrosymmetric oxides nanowires, npj Quantum Mater. **7**, 2 (2022).
[56] M. T. Mercaldo, P. Solinas, F. Giazotto, and M. Cuoco, Electrically tunable superconductivity through surface orbital polarization, Phys. Rev. Appl. **14**, 034041 (2020).
[57] L. Bours, M. T. Mercaldo, M. Cuoco, E. Strambini, and F. Giazotto, Unveiling mechanisms of electric field effects on superconductors by a magnetic field response, Phys. Rev. Res. **2**, 033353 (2020).
[58] M. T. Mercaldo, F. Giazotto, and M. Cuoco, Spectroscopic signatures of gate-controlled superconducting phases, Phys. Rev. Res. **3**, 043042 (2021).
[59] G. De Simoni, S. Battisti, N. Ligato, M. T. Mercaldo, M. Cuoco, and F. Giazotto, Gate control of the current–flux relation of a Josephson quantum interferometer based on proximitized metallic nanojuntions, ACS Appl. Electron. Mater. **3**, 3927 (2021).
[60] M. T. Mercaldo, C. Ortix, and M. Cuoco, High orbital-moment Cooper pairs by crystalline symmetry breaking, Adv. Quantum Technol. **6**, 2300081 (2023).
[61] Y. Fukaya, S. Tamura, K. Yada, Y. Tanaka, P. Gentile, and M. Cuoco, Interorbital topological superconductivity in spin-orbit coupled superconductors with inversion symmetry breaking, Phys. Rev. B **97**, 174522 (2018).
[62] Y. Fukaya, K. Yada, Y. Tanaka, P. Gentile, and M. Cuoco, Orbital tunable $0-\pi$ transitions in Josephson junctions with noncentrosymmetric topological superconductors, Phys. Rev. B **102**, 144512 (2020).
[63] Y. Fukaya, Y. Tanaka, P. Gentile, K. Yada, and M. Cuoco, Anomalous Josephson coupling and high-harmonics in noncentrosymmetric superconductors with *S*-wave spin-triplet pairing, npj Quantum Mater. **7**, 99 (2022).
[64] A. Gurevich, Enhancement of the upper critical field by nonmagnetic impurities in dirty two-gap superconductors, Phys. Rev. B **67**, 184515 (2003).
[65] I. O. Kulik and A. N. Omel'yanchuk, Contribution to the microscopic theory of the Josephson effect in superconducting bridges, Pis'ma Zh. Eksp. Teor. Fiz. **21**, 216 (1975) [JETP Lett. **21**, 96 (1975)].
[66] A. A. Golubov, M. Y. Kupriyanov, and E. Il'ichev, The current-phase relation in Josephson junctions, Rev. Mod. Phys. **76**, 411 (2004).
[67] Single-band superconductor stands here for the sake of simplicity for any conventional superconductor with a high enough transition temperature, including also multi-band superconductors with attractive inter-band interactions, in particular, including MgB_2 and the A15-compounds mentioned below in the text. They should be treated then within an effective one-band approximation.
[68] V. Grinenko, P. Materne, R. Sarkar, H. Luetkens, K. Kihou, C. H. Lee, S. Akhmadaliev, D. V. Efremov, S.-L. Drechsler, and H.-H. Klauss, Superconductivity with broken time-reversal symmetry in ion-irradiated $Ba_{0.27}K_{0.73}Fe_2As_2$ single crystals, Phys. Rev. B **95**, 214511 (2017).
[69] J. Garaud, M. Silaev, and E. Babaev, Change of the vortex core structure in two-band superconductors at the impurity-scattering-driven $s_{\pm}/s_{++}$ crossover, Phys. Rev. B **96**, 140503(R) (2017).
[70] Y. Yerin, S.-L. Drechsler, M. Cuoco, and C. Petrillo, Magneto-topological transitions in multicomponent superconductors, Phys. Rev. B **106**, 054517 (2022).
[71] Y. V. Sharvin, A possible method for studying Fermi surfaces, ZhETF **48**, 984 (1965) [Sov. J. Exper. Theor. Phys. **21**, 655 (1965).
[72] A. A. Zubkov, M. Y. Kupnyanov, and V. K. Semyonov, Stationary properties of Josephson junctions with direct conductivity (in Russian), Fiz. Nizk. Temp. **7**, 1365 (1981).
[73] Y. S. Yerin and A. N. Omelyanchouk, Josephson currents in point contacts between dirty two-band superconductors, Low Temp. Phys. **36**, 969 (2010).
[74] Y. Yerin and A. N. Omelyanchouk, Proximity and Josephson effects in microstructures based on multiband superconductors, Low Temp. Phys. **43**, 1013 (2017).
[75] I. Kulik and A. N. Omelyanchouk, Josephson effect in superconducting bridges: microscopic theory (in Russian), Fiz. Nizk. Temp. **4**, 296 (1978).
[76] A. Buzdin and A. E. Koshelev, Periodic alternating 0- and π-junction structures as realization of φ-Josephson junctions, Phys. Rev. B **67**, 220504(R) (2003).
[77] A. I. Buzdin, Proximity effects in superconductor-ferromagnet heterostructures, Rev. Mod. Phys. **77**, 935 (2005).
[78] Y. Fukaya, M. T. Mercaldo, D. Margineda, A. Crippa, E. Strambini, F. Giazotto, C. Ortix, and M. Cuoco, Design of supercurrent diode by vortex phase texture, arXiv:2403.04421.
[79] Z. Huang and X. Hu, Josephson effects in three-band superconductors with broken time-reversal symmetry, Appl. Phys. Lett. **104**, 162602 (2014).

[80] Y. S. Yerin and A. N. Omelyanchouk, Frustration phenomena in Josephson point contacts between single-band and three-band superconductors, Low Temp. Phys. **40**, 943 (2014).

[81] Y. S. Yerin, A. S. Kiyko, A. N. Omelyanchouk, and E. Il'ichev, Josephson systems based on ballistic point contacts between single-band and multi-band superconductors, Low Temp. Phys. **41**, 885 (2015).

[82] C. Xu, W. Yang, and C. Wu, Frustrated superconducting junction with tricomponent pairing gap functions, Phys. Rev. B **108**, 094509 (2023).

[83] C. Guarcello, L. Chirolli, M. T. Mercaldo, F. Giazotto, and M. Cuoco, Frustration-driven Josephson phase dynamics, Phys. Rev. B **105**, 134503 (2022).

[84] Y. Yerin, A. Omelyanchouk, S.-L. Drechsler, D. V. Efremov, and J. van den Brink, Anomalous diamagnetic response in multiband superconductors with broken time-reversal symmetry, Phys. Rev. B **96**, 144513 (2017).

[85] A. Greco, Q. Pichard, E. Strambini, and F. Giazotto, Double loop dc-SQUID as a tunable Josephson diode, arXiv:2404.05521.